Chapter

Observation and Analyses of Coulomb Crystals in Fine Particle Plasmas

Yasuaki Hayashi

Abstract

Observations of crystal-like ordering of fine particles in plasmas were first reported in 1994, when we succeeded to observe it by growing carbon fine particles in a methane plasma. Video cameras and Mie-scattering ellipsometry were applied for the analyses of fine particles and their crystal ordering. 3D and 2D crystal structures were observed for smaller and larger particles, respectively. The former structures were fcc, fco, and bct, but bcc structure was not observed. The result is due to the fact that the rearrangement from fcc to fco or bct occurs with both constant particle density in horizontal planes and constant interplane vertical distance. Behaviors of fine particles under microgravity were observed and analyzed using ready-made and injected fine particles. Its experimental result showed that the resultant force composed of electrostatic and ion drag forces pushes fine particles outward from the center forming a void.

Keywords: fine particle plasma, fine particle, plasma, Coulomb crystal, ellipsometry, Mie scattering, Mie-scattering ellipsometry, dusty plasma, microgravity, one-component plasma, strongly coupled plasma

1. Introduction

Observations of crystal-like ordering of fine particles in plasmas were first reported in 1994 [1–4]. They were performed by growing carbon particles in a methane plasma [1], silica particles growing in plasma [2], and ready-made polymer particles in argon plasmas [3, 4]. The possibility of observation of crystal-like ordering of fine particles, which was called Coulomb solid or Coulomb crystal, in a low-pressure plasma was predicted through calculation by Ikezi [5]. It was similar to those in the solution of colloids generally negatively single-charged, while micron-sized fine particles get thousands of electrons or more on their surface in a plasma. They can form solid state easily because of larger value of the Coulomb-coupling parameter, Γ, as follows:

$$\Gamma = \frac{(eQ)^2/4\pi\varepsilon_0 a}{k_B T}, \tag{1}$$

where e, Q, a, and T are the unit charge, the number of electron charge per one particle, the Wigner-Seitz radius, and absolute temperature, respectively. The numerator and denominator of Eq. (1) are the average Coulomb energy and the kinetic energy of a fine particle, respectively. In the case that $a \gtrsim \lambda_D$, where λ_D is

the Debye length, the Yukawa-type interaction works and the Coulomb-coupling parameter is replaced with Γ^* defined as

$$\Gamma^* = \Gamma e^{-a/\lambda_D} = \frac{(eQ)^2/4\pi\varepsilon_0 a}{k_B T} e^{-a/\lambda_D,} \tag{2}$$

Charge neutrality is satisfied in a fine particle plasma as

$$-N_d Q + (n_i - n_e) = 0, \tag{3}$$

where N_d, n_i, and n_e are the density of fine particles, ions, and electrons, respectively. The first term of the left side of Eq. (3), $-N_d Q$, is negative and $N_d Q$ is balanced with the positive second term, $(n_i - n_e)$. Since an ion and an electron have much smaller mass and higher mobility than a fine particle, it is suggested that the part $(n_i - n_e)$ acts as background field equivalently. This means that negatively charged fine particles are surrounded by the positive background. Such a system is called one-component plasma [6]. As with charged particles, neutral atoms or molecules act on fine particles as background temperature environment. The friction to fine particles by neutral atoms or molecules decreases the temperature T in Eq. (1) or Eq. (2).

The physics of one-component plasma or strongly coupled plasma has been studied mainly by computer simulation such as the Monte Carlo method and molecular dynamics since 1957, when the liquid–solid phase transition by hard spheres in a confined condition was discovered by Alder and others [7–9]. Following this study, the phase transitions were confirmed using other repulsive potentials such as Coulomb [10], soft sphere [11], and Yukawa [12, 13].

Although theoretical or computer-simulation studies on one-component plasma and strongly coupled plasma have been proceeded, there are not many experimental studies except for the use of ion trap or colloidal solutions. Ions confined in a Pawl or Penning trap can form crystal ordering [14, 15]. Colloids in electrolyte solution form crystal structures [16]. However, special skills and time are required for the formation. Compared to that, Coulomb crystals in fine particle plasma are formed more easily and quickly.

In this chapter, the formation, observation, and analysis of Coulomb crystals in fine particle plasmas are presented. Current status of their application to study of solid state physics phenomena is also described.

2. Formation and observation of Coulomb crystal in fine particle plasmas

2.1 Formation of Coulomb crystal

Coulomb crystals in fine particle plasmas have been formed typically under the conditions as shown in **Table 1**.

Figure 1 shows an example of a plasma system for Coulomb crystal formation [17]. The system is a parallel-plate 13.56-MHz radio-frequency (RF) plasma device, which includes eight pieces of permanent magnets in the RF electrode to generate planar-magnetron plasma. Discharge gas is introduced and evacuated far from the area of center of vacuum chamber in order that fine particles are suspended under a stagnant condition to reduce the effect of gas drag. A side view of suspended fine particles above the RF electrode is shown in **Figure 2**. In this case, fine particles of spherical divinylbenzene polymer 2.74 μm in diameter were injected into argon plasma under the pressure of 65 Pa and RF power of 2 W.

Fine particles	Material	Polymer, silica, carbon
	Shape	Sphere
	Size	1–10 μm
	Size distribution	Monodisperse
Discharge device	Power supply	RF (13.56 MHz), DC
	Electrode type	Parallel-plate
Plasma conditions	Discharge gas	Argon, helium, methane
	Pressure	10–100 Pa
	Discharge power	As low as limit of particle suspension

Table 1.
Typical conditions for Coulomb crystal formation in plasma.

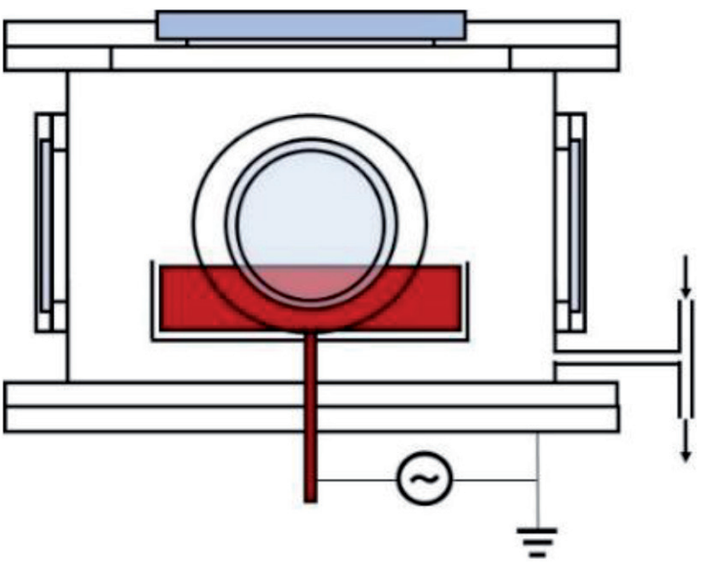

Figure 1.
Schematic view of plasma system for Coulomb crystal formation. Dark red and light blue parts show RF electrode and viewing glass windows, respectively. Other parts are grounded.

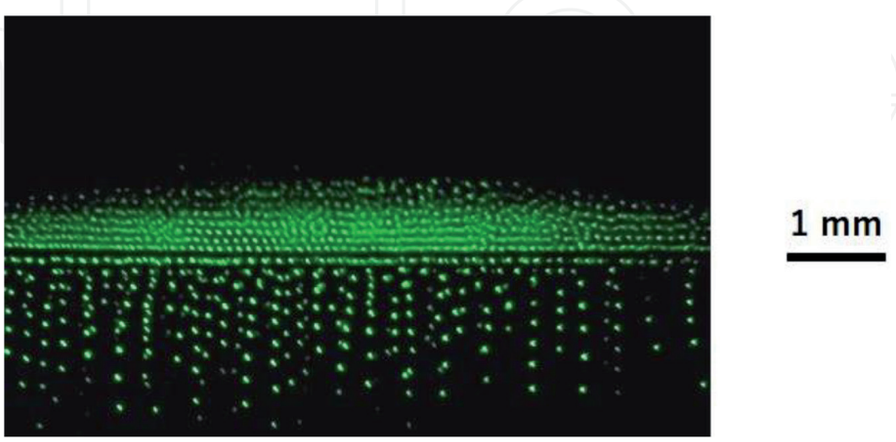

Figure 2.
Side view of arrangement of fine particles above RF electrode.

The arrangement of fine particles in **Figure 2** is divided up and down. The upper part of fine particles forms horizontal planes, while the lower part forms vertical strings. It is judged that the border of the two particle arrangements corresponds

to the plasma-sheath boundary. It was explained by theoretical analysis [18] and computer simulation [19] that the vertical particle string of fine particles in the lower part is created by ion-wake field, which is effective in the region of ion speed more than Mach sound velocity, that is, in the sheath region. When the particle strings are closely packed, they form a two-dimensional (2D) hexagonal structure. Meanwhile, the horizontal layers of fine particles in the upper part are formed under the one-dimensional (1D) compressive force in the vertical direction [20]. Fine particles are arranged closely packing in each plane. To minimize the free energy in three-dimension (3D), such particles tend to be staggered with those in the next layer forming 3D close-packed structures: hexagonal close-packing (hcp) or face-centered cube (fcc). In this way, fine particles can form a 2D hexagonal structure and 3D structures such as fcc and hcp. The possibility of formation of body-centered cubic (bcc) structure will be described in Section 2.2.

2.2 Observation of Coulomb crystal

Coulomb crystals can be observed by laser light scattering. When a visible light laser is used, light scattering from micron-sized fine particle is in the Mie-scattering regime. In such a regime, fine particles can be individually observed by the scattered laser light of output power of even a few mW when they are in the arrangement of solid-like state.

3D structures of Coulomb crystal were observed by the use of plasma system as shown in **Figure 3**. The system consists of a vacuum reaction chamber, a blue argon-ion laser (wavelength: 488 nm, 100 mW output power), and two CCD video cameras, and a rotating analyzer for Mie-scattering ellipsometry [21]. In case of confirmation of the position of fine particles in the vertical direction, a red diode laser (wavelength: 690 nm, 20 mW output power) was also used. The light beam of the diode laser was expanded perpendicular to the RF electrode with the use of a cylindrical lens.

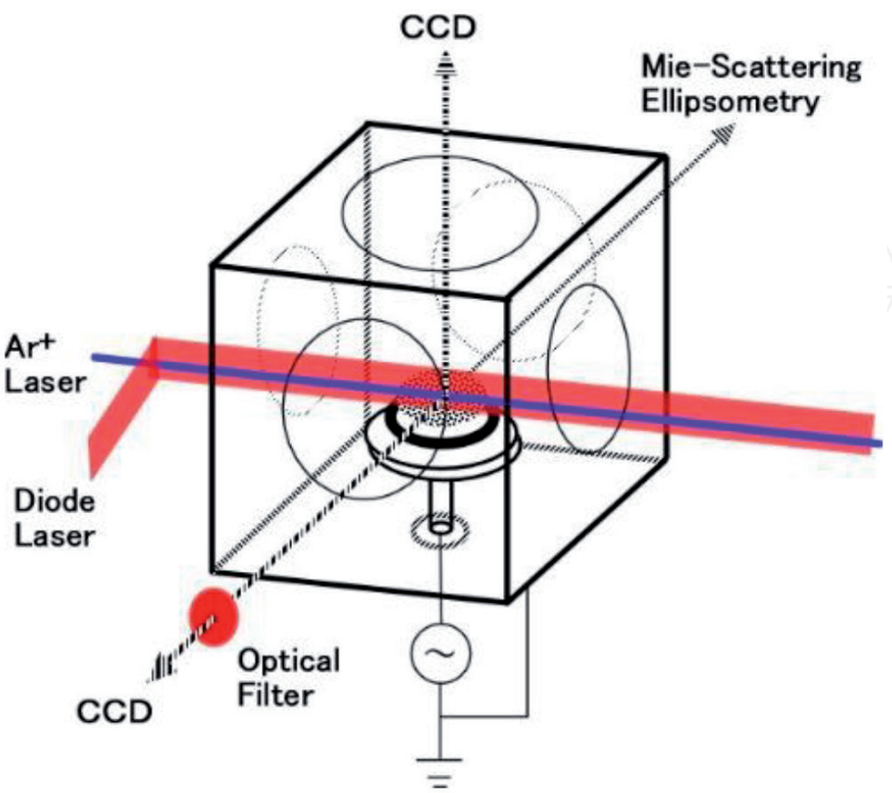

Figure 3.
Schematic of plasma system for observation of 3D structure of Coulomb crystal [21].

The vacuum chamber is a cube with a side length of 10 cm. Viewing windows are provided in the five faces of the chamber. Two are for the incidence and outgoing of laser light. Two others are for the observation of Coulomb crystals from the side and the top. The other one is for the monitoring of the particle diameter by Mie-scattering ellipsometry. RF of 13.56 MHz was applied to an electrode of 4 cm diameter with the chamber wall grounded. A ring of 3 cm inner diameter was put on the electrode in order to effectively trap fine particles above it by forming a potential bucket. Gas inlet and exhausting ports were provided close to each other so that particles were not transported by gas flow.

Fine particles were prepared by film growth on the seeds of ultrafine carbon particles, which were injected at the first stage of the growth, in a 20% methane/argon plasma under the conditions of 5 W RF power and 40 Pa (0.3 Torr) pressure. Spherical and monodisperse carbon particles can be grown through coating of hydrogenated amorphous carbon on the seeds by the dissociation of methane gas in the plasma [22]. Using Mie-scattering ellipsometry, the diameter of growing particles was monitored, and the growth was stopped by the decrease of RF power to 1 W for the particles of diameter of 1.4 μm, with which three-dimensional Coulomb crystals were formed in the experiments that will be shown in Section 3.2.

Fine particles spread over the entire region in the potential bucket are suspended about 5 mm above the electrode in the luminous plasma region of the negative glow. The top and side images, which were taken at the same position and at the same time by irradiation with blue laser light only, of a 3D Coulomb crystal formed by 1.4-μm carbon particles are shown in **Figure 4** [23]. The relative horizontal positions of fine particles in the top view were adjusted so as to agree with those in the side view at a crystal-grain boundary. Bright spots in the top view image indicate particles in the lowest layer and comparatively dimmed or small spots indicate those in the second lowest layer, because particles were illuminated in the off axis of the laser beam of the Gaussian distribution under them. From the correspondence of particle arrangement in the top view with that in the side view, particles are found to be aligned in the perpendicular direction of

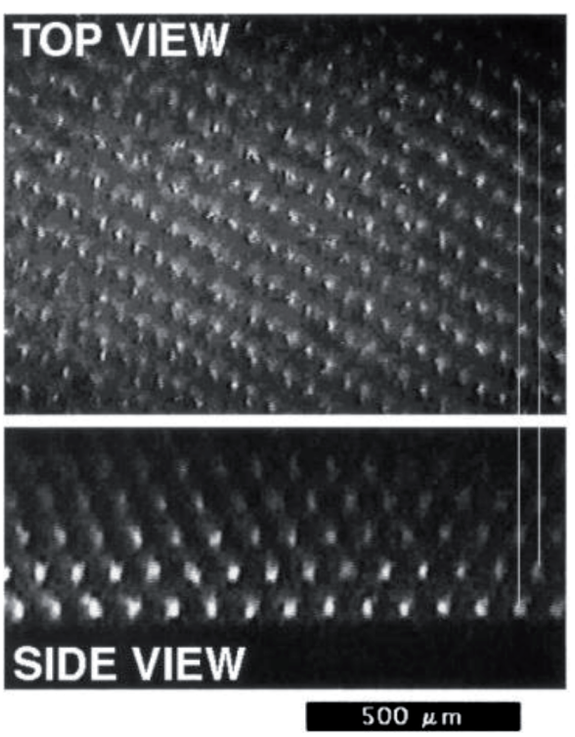

Figure 4.
Top and side video images of a 3D Coulomb crystal taken at the same time and the same position [23].

the side view plane. This means that each bright spot in the side view shows particles piled up in the direction (see the lines on the right in the figure).

It can be seen that the crystal structure in **Figure 4** is similar to the body-centered cubic (bcc) structure with (110) planes parallel to the electrode. The three-dimensional structure of a unit cell of the crystal is depicted in **Figure 5**. The lattice constants a, b, and c are determined from the average in the image to be 106, 157, and 165 mm, respectively. The relation among these sizes is $\sqrt{2}\ a < b \leq c$; therefore, the crystal structure is not strictly body-centered cubic (bcc) but body-centered tetragonal (bct) or generally face-centered orthorhombic (fco). The top view and the side view in **Figure 4** show (001) planes and planes perpendicular to [110] axes of the structure, respectively.

3D observation of the change of structure of Coulomb crystal was carried out. **Figure 6** shows the top and side views of change of fine particles arrangement every 1/3 s. As the blue argon-ion laser beam runs through the lower region of fine particles and the scattered blue light is more intensive than the scattered red diode-laser light, the particle arrangement in a few lowest layers was distinguished in top views. Side views were taken by the use of another CCD video camera with an optical band-pass filter for the red light (690 nm) put in front of it. Therefore particles in a few vertical layers were observed by the latter CCD camera.

The crystal structure of stage "A" in **Figure 6** was analyzed to be fco or bct, while that of stage "D" was fcc [21]. Change from "A" to "D" in the side view indicates that from the crystal observation axis of bct[100] to fcc[110] for, and change from "A" to "D" in the top view shows that from bct[110] to fcc[111]. The change of inclination of particle rows in the vertical direction is clearly seen in the side view. Corresponding to the side view, the particle arrangement in horizontal layers shown in the top view changes in the way that particles in the third lowest layer, which are indicated by very dimmed spots, gradually separate from the particle positions in the lowest layer. The change of crystal structure is illustrated in **Figure 7**.

The results of the observation of the time and space changes of 3D Coulomb crystal structures suggest that the structural transitions occurred by the slip of crystal planes parallel to the electrode. The slip planes were fcc(111) and bct(110). In the martensitic transformation of metallic iron, the slip of crystal planes generally occurs between fcc(111) and bcc(110) or bct(110) [24]. The structural transitions of 3D Coulomb crystals in dusty plasmas well matches those of real metallic crystals.

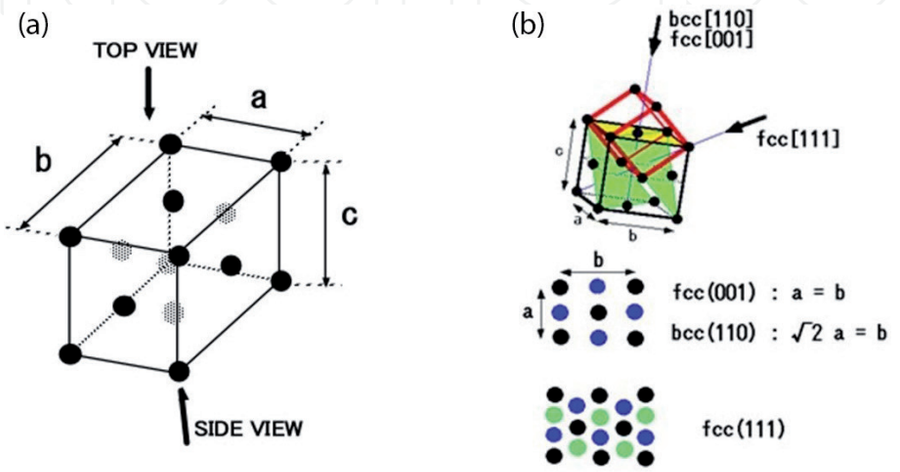

Figure 5.
3D crystal structures of bcc, bct, or fco (a) [23]; bcc and fcc (b) [21].

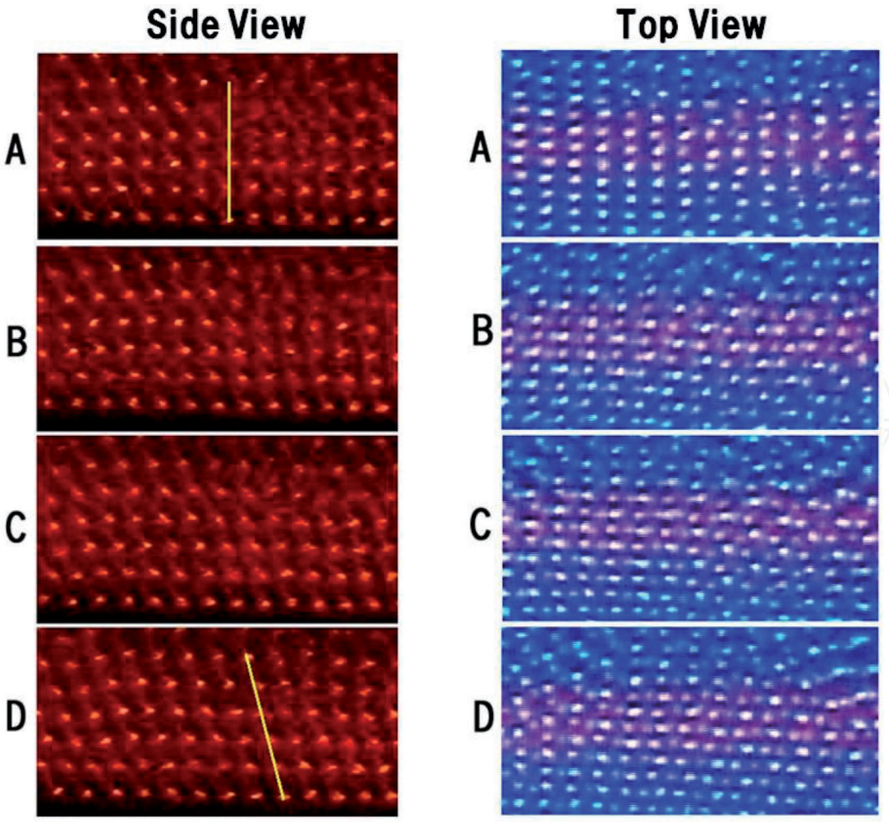

Figure 6.
Structural transition of Coulomb crystal every 1/3 s from A to D. Side and top views were taken at the same time. Fine particles in the red colored regions in the top view correspond to those in the side view [21].

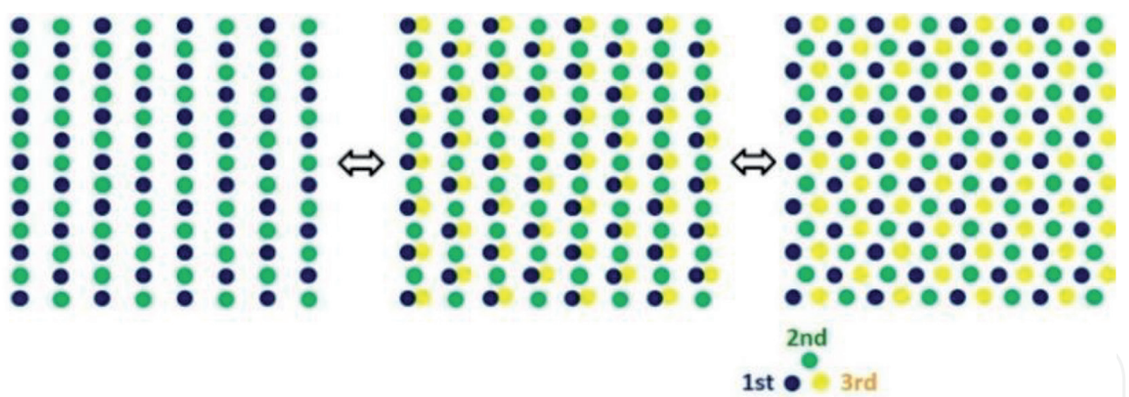

Figure 7.
Illustration of structural change of Coulomb crystal between bct (fco) and fcc from top view. Fine particles in the first, second, and third lowest layers are indicated by dark (blue), pale (green), and light (yellow) circles, respectively.

When a crystal structure simply changes by slip of crystal planes from fcc to another cubic structure, the relation between two horizontal lattice constants should hold as $a : b = 1: \sqrt{3}$ (=1.73). If the crystal rearranges its structure for 3D minimum Coulomb energy, the structure changes to bcc with (110) planes parallel to an electrode for $a : b = 1: \sqrt{2}$ (=1.41). The b/a ratio of the crystal in **Figure 4** is about 1.5. This discrepancy can be explained by the fact that the particle arrangement is reconstructed for 2D minimum Coulomb energy with constant particle density in horizontal planes and with interplane vertical distance constant [21, 23]. It is suggested that the crystal structure was formed from the pile of the plain layers perpendicular to the direction of an external force with constant interplane distance, which was also shown by molecular dynamics simulation [20], being arranged by

the secondary effect of Coulomb force of particles in nearby layers to minimize average Coulomb energy [23].

3. Analyses of behavior of fine particles in plasmas

3.1 Analysis by polarized light scattering

The intensity of light scattered by a single spherical particle is calculated through the Mie-scattering theory [25, 26] when the diameter, D, and refractive index, m, of a particle are given. For multiple monodisperse particles, the scattered light intensity is proportional to the number of particles, N_d. Thus the scattered light intensity depends on both D and N_d. In order to determine D and N_d separately, the measurement of polarization of scattered light is required simultaneously.

The complex scattering amplitude functions, $\boldsymbol{S_s}$ of a polarization component perpendicular to the scattering plane and $\boldsymbol{S_p}$ of a parallel one, are defined by the following equations:

$$\boldsymbol{S_s} = \sum_{n=1}^{\infty} \frac{2n+1}{n(n+1)} \{\boldsymbol{a_n}\pi_n(cos\theta) + \boldsymbol{b_n}\tau_n(cos\theta)\}, \tag{4}$$

$$\boldsymbol{S_p} = \sum_{n=1}^{\infty} \frac{2n+1}{n(n+1)} \{\boldsymbol{b_n}\pi_n(cos\theta) + \boldsymbol{a_n}\tau_n(cos\theta)\}, \tag{5}$$

where $\boldsymbol{a_n}$ and $\boldsymbol{b_n}$ are expressed with the Bessel functions including the diameter D and complex refractive index $\boldsymbol{m}$ of a fine particle; π_n and τ_n are expressed with the Legendre polynomials as functions of scattering angle θ [27, 28]. The absolute value of ratio, $|\boldsymbol{S_p}/\boldsymbol{S_s}|$, can be determined for monodisperse fine particles with known refractive index with the use of three polarizing elements: one placed in position before scattering and the other two placed after scattering with polarization azimuth angles parallel and perpendicular to the scattering plane [29]. The value of $|\boldsymbol{S_p}/\boldsymbol{S_s}|$ does not depend on particle number N_d but only on diameter D. Thus D is determined first and then N_d is determined from the intensity of scattered light after calibration.

3.2 Analysis by Mie-scattering ellipsometry

In an analogous way to the reflection ellipsometry, angle parameters for Mie scattering are defined from the ratio between two complex scattering amplitude in the direction parallel and perpendicular to the scattering plane. When particles are spherical and monodisperse, the ellipsometric parameters Ψ and Δ are defined by the ratio of the scattering amplitude functions of $\boldsymbol{S_s}$ and $\boldsymbol{S_p}$ [30], which are complex numbers, as

$$\tan\Psi e^{i\Delta} = \frac{\boldsymbol{S_p}}{\boldsymbol{S_s}}. \tag{6}$$

It is obvious that $\tan\Psi = |\boldsymbol{S_p}/\boldsymbol{S_s}|$, which can be determined also by the method described in Section 3.1. Another value of parameter, Δ, is added as information about fine particles in Mie-scattering ellipsometry. When particles are polydisperse in the size range of Mie scattering, the scattered light generally results in some depolarization even if the incident light is fully polarized [31]. In this case, the Stokes vector and the Mueller matrix are required for the calculation of polarization state. Details about the analysis of fine particles by Mie-scattering ellipsometry are described in Refs. [30, 32, 33].

Figure 8 shows a (Ψ, Δ) trajectory as a result of Mie-scattering ellipsometry measurement for spherical carbon particles growing by coating in a plasma including methane (**Figure 8(A)**). The time evolution of diameter and density of fine particles are obtained from correspondence of graphs of (a) and (b) in **Figure 8(B)** as shown in **Figure 9** [1].

The transitions of arrangement of fine particles during the growth in a methane/helium plasma under the conditions of pressure of 106 Pa (0.8 Torr) and RF power of 5 W are shown in **Figure 10** [34]. By Mie-scattering ellipsometry, particle diameter was evaluated as 1.3, 1.7, 2.2 μm at 30, 45, and 80 min, respectively.

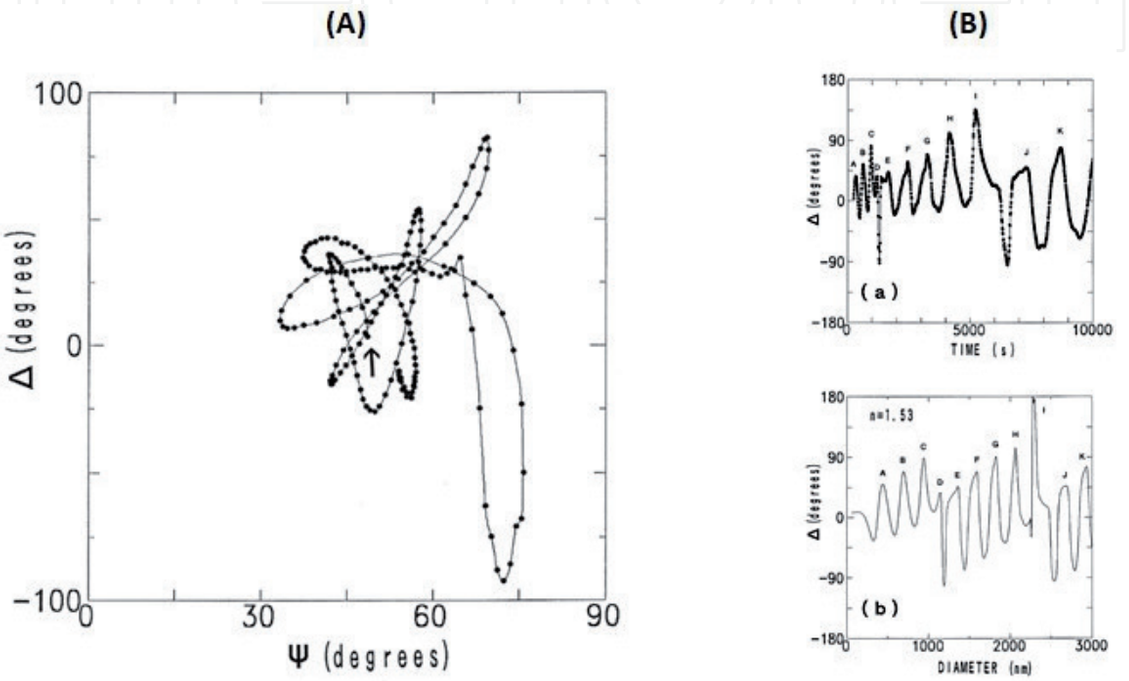

Figure 8.
Experimental result of evolution of ellipsometric parameters, (Ψ, Δ), during carbon particle growth. (A); (a) time evolution of Δ by experiment, (b) size evolution of Δ by simulated calculation (B) [1].

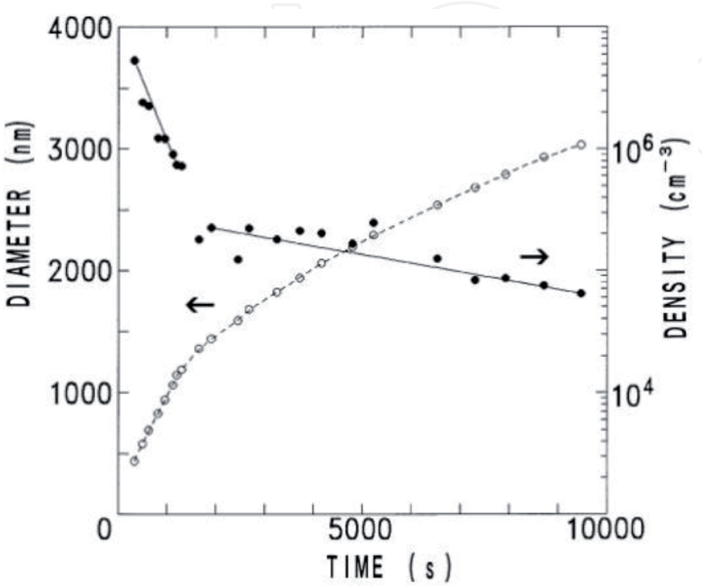

Figure 9.
Time evolution of particle diameter (open circles and broken curves) and density (closed circles and solid lines) [1].

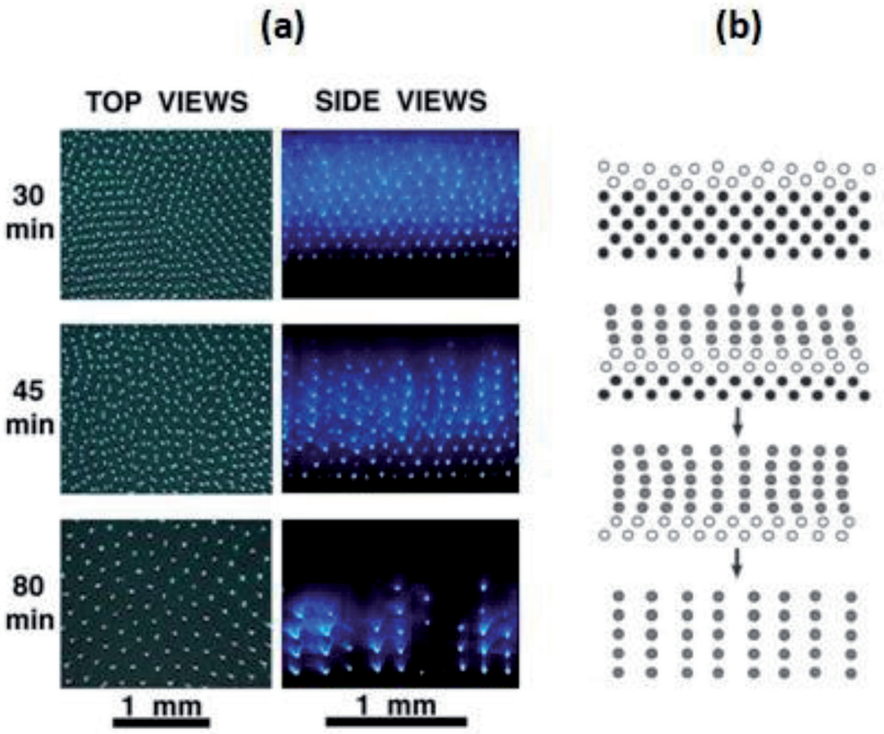

Figure 10.
Changes of top and side views of particle arrangement (a). The particles of top views are in the two lowest layers and those of side views in several lowest layers. Illustrations of change of side-view particle arrangement are shown (b) [34].

The particle arrangement at 30 min shows 3D regularity in the lowest four or five horizontal layers, especially crystal-like ordering in the lowest two layers. It is seen at 45 min that particles tend to be weakly chained in the vertical direction in the upper region. In its video movie, the chains were slowly swinging from right to left. The top view shows that particles in the lowest layer are randomly arranged. At 80 min, the particles are aligned like stiff rods in the vertical direction. They seem to form a close-packed 2D crystal, that is, hexagonal crystal. The structures of arrangement of smaller and larger particles correspond to those of upper and lower parts in **Figure 2**, respectively. However, the crystal edge of the 2D crystal is seen at the lowest side in the side view in **Figure 10**, while it is seen at the top side of 2D structure, which is the boundary between 2D and 3D structures, in **Figure 2**.

The spatial distribution of size of arranged particles under the same conditions as shown in **Figure 2** was analyzed by Mie-scattering ellipsometry using an image sensor instead of a photo-detector [35, 36]. Determined ellipsometric parameters are plotted on the Ψ-Δ coordinate plane, as shown in **Figure 11**, along with the trajectory obtained by calculation for spherical particles of refractive index of 1.56, the scattering angle of 88°, and diameter of 2650–2830 nm for each 10 nm. It should be noted that the trajectory shows a significant change with the diameter. The calculated trajectory was obtained for the best fitting to the determined values. By the comparison of the determined values Ψ and Δ with calculation, the size was evaluated to be 2.70, 2.74, 2.75, and 2.77 μm for particles in upper to lower layers (L4 to L1). Thus larger particles sank in lower position. However, although interlayer distance was observed to be about 100 μm, the distance between force balance positions for isolated 2.74 and 2.75 μm fine particles calculated in a way as

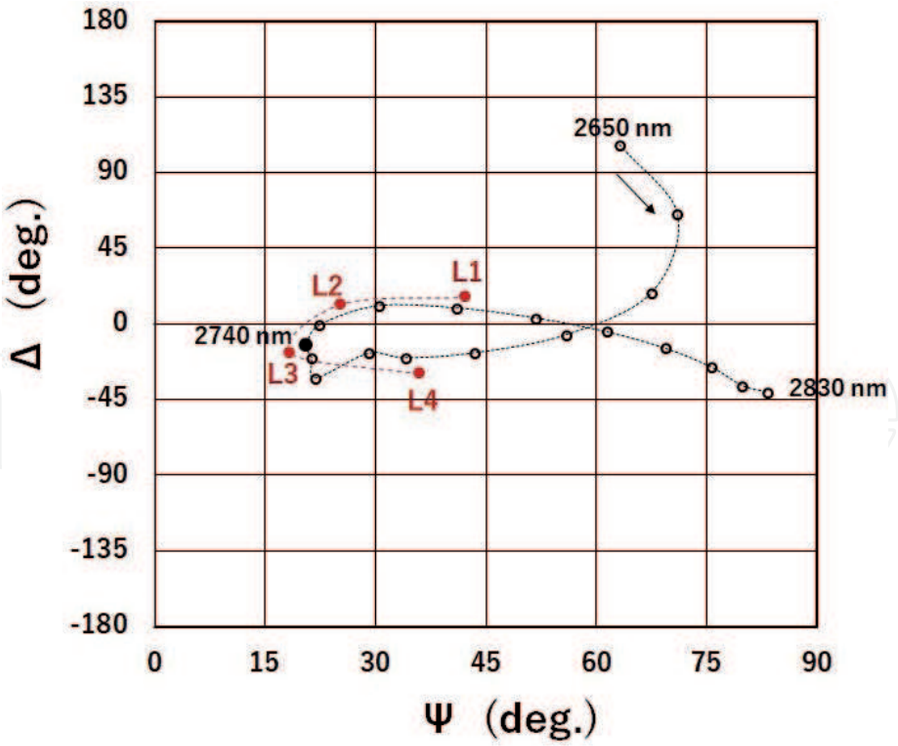

Figure 11.
Ellipsometric parameters of measurement for fine particles in layers upper to lower: L1, L2, L3, L4 (closed circles and dotted line) and calculation for spherical particles of refractive index of 1.56 and diameter of 2650–2830 nm for each 10 nm (open circles and solid line).

shown in Section 4.2 is one order of magnitude smaller than the observed interlayer distance. The interlayer distance of 100 μm must be due to mutual Coulomb repulsion. The reason why larger particles exist in lower layers is explained as follows.

The total chemical potential $\mu = \mu_{\text{int}} + \mu_{\text{ext}}$, where μ_{int} is the internal chemical potential and μ_{ext} is the external potential mainly due to gravity and electrostatic fields, has a constant value in the system of thermal equilibrium. Since μ_{int} is proportional to the logarithm of concentration ratio,

$$c = c_0 \exp\left(-\mu_{\text{ext}}/k_{\text{B}}T\right), \tag{7}$$

where c and c_0 are particle concentration and a constant, respectively. The gravitational force is proportional to the third power of the diameter D of fine particle, while electrostatic force is proportional to the diameter. Then, μ_{ext} above the plasma-sheath boundary is related to the equation (see Section 4),

$$\begin{aligned} \mu_{\text{ext}} &= m\,\text{g}\,z - \int (eQE)dz \\ &\cong a\,z\,D^3 - b\left(\int Edz\right)D \\ &\cong a\,z\,D^3, \end{aligned} \tag{8}$$

where m, g, z, and E are particle mass, the gravitational constant, vertical coordinate value, and the electrostatic field strength, respectively; a and b are constants independent of z and D. The external potential is larger for larger particles. Thus, larger particles moved to lower position according to the thermal equilibrium in several minutes after injection.

4. Forces acting on fine particle

4.1 Suspension of fine particle in plasma by force balance

Fine particles are suspended mainly at the balanced position of electrostatic force (f_E), ion drag force (f_I), and gravity (f_G). When they are distributed between two parallel-plate electrodes with central axes in vertical direction, the upward resultant force of $f_E - f_I - f_G$ acts on them near the lower electrode while that of $f_I - f_E - f_G$ acts on them near the upper electrode. These three forces are related with particle diameter, D, by the following equations,

$$f_E = e(rD)E, \tag{9}$$

$$f_I = n_i V_s m_i V_i \pi\left(b_c^2 + 4b_R^2 \ln\Lambda\right), \tag{10}$$

$$f_G = \pi\rho D^3/6, \tag{11}$$

where r is the particle charge number per unit size of particle diameter D: rD is the particle charge number, E is the electric field, n_i is the ion density, V_i is the ion drift velocity, $V_s = \sqrt{(V_i^2 + V_{iT}^2)}$ is the ion velocity (V_{iT} is the ion thermal velocity), m_i is the mass of ion, b_c is the impact parameter of ion orbit grazing particle, b_R is the impact parameter of right-angle-scattering ion orbit, $\ln\Lambda$ is the Coulomb logarithm, and ρ is the mass density [37].

The three forces were calculated under the following simple assumptions: r = 10^9 /m; E = 500 V/m; n_i = 10^{14} /m^3; V_i = 2000 m/s; V_{iT} = 1500 m/s; m_i = 10^{-26} kg; b_c ≈ $D/2$; $b_R \approx 4D$, $\ln\Lambda \approx 10$; ρ = 2*10^3 kg/m^3. The variations of the forces with particle diameter are indicated by a log-log graph in **Figure 12**. f_E, f_I and f_G are proportional to D, D^2 and D^3, respectively.

Ion drag force could be larger than that calculated by Eq. (10) [37] because of more widespread ion-particle interaction beyond the Debye-length, which will be described in Section 4.2.

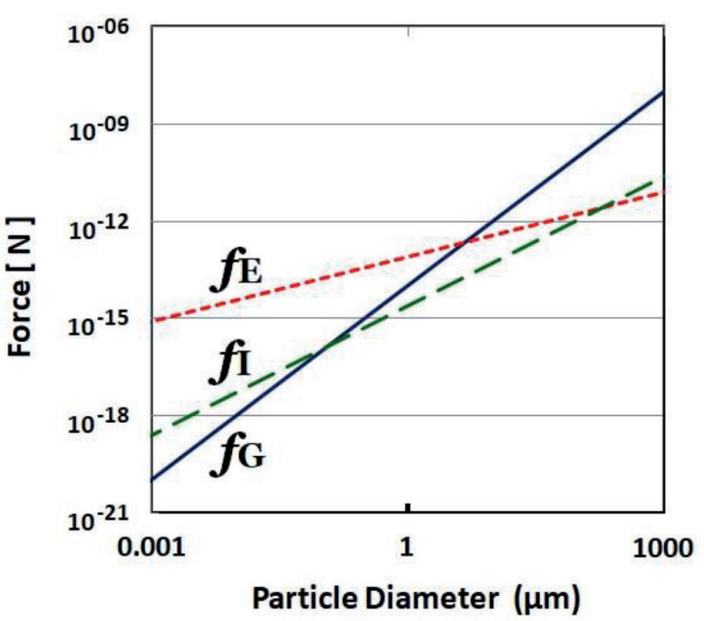

Figure 12.
Variation of electrostatic force (fE), ion-drag force (f_I), and gravity (f_G) with particle diameter.

4.2 Fine particle behavior under microgravity

As was described in Section 4.1, the electrostatic, ion drag, and gravitational forces act on fine particles. The gravitational force pulls fine particles downward. When fine particles are suspended in a plasma generated between two parallel plates placed horizontally, they sink around the lower plasma-sheath boundary. If gravitational force is extremely decreased or lost, the position of force balance changes. Thus, microgravity experiments should be useful for analyzing forces acting on fine particles in a plasma.

A parallel-plate RF plasma system was used for the experiments (**Figure 13**) [38]. A piezoelectric vibrator for the injection of fine particles into a plasma was contained in an RF electrode, which was put at the bottom of vacuum chamber of the system. The top of the electrode is covered with a grid so that fine particles can be pushed up. A grounded counter electrode is placed at the upper side of the RF electrode at the distance of 14 mm with a vertically symmetric structure. The outer diameter of the two electrodes is 40 mm and the gap space of the electrodes is surrounded by a transparent plastic cylinder with an inner diameter of 35 mm. The vacuum chamber is shaped octagonal and has six viewing windows: one for the entrance of the laser light, another for the exit, and the other four for observation of the arrangement of fine particles using scattered laser light. Using two charge-coupled device (CCD) video cameras placed in front of two of the four windows, the XYZ-3D position of each fine particle can be determined.

Spherical divinylbenzene fine particles 2.27 ± 0.10 μm in diameter were put into the piezoelectric vibrator. The density of the fine particle is 1.19 g/cm^3, and the weight is 7.29×10^{-12} gw. Helium gas was introduced at the pressure of 133 Pa (1 Torr). After plasma was generated with the RF power of 2 W, fine particles were pushed up into the plasma. When a sufficient quantity of fine particles was introduced into the plasma, the vibrator was switched off and then the experimental system was placed in a microgravity environment.

Figure 14 shows images taken using the Y-axis video camera before and during the microgravity condition of less than 10^{-4} G (gravity constant) that was generated in a capsule of drop tower for 4.5 s at the Micro-Gravity Laboratory (MGLAB) at Toki in Japan. The number of injected fine particles was approximately 30,000. A diode laser, which radiates light 690 nm in wavelength, was used for the observation of fine particles by scattered laser light. The image obtained immediately before the

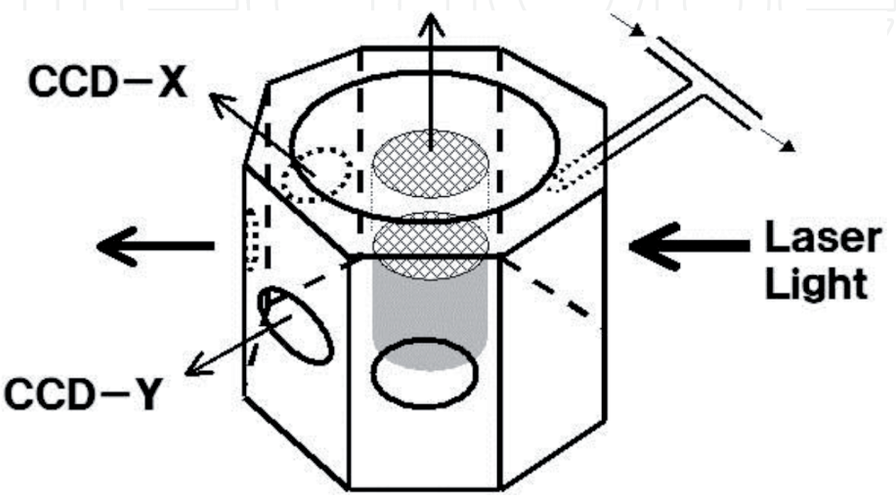

Figure 13.
Schematic of parallel-plate RF plasma system for microgravity experiment [38].

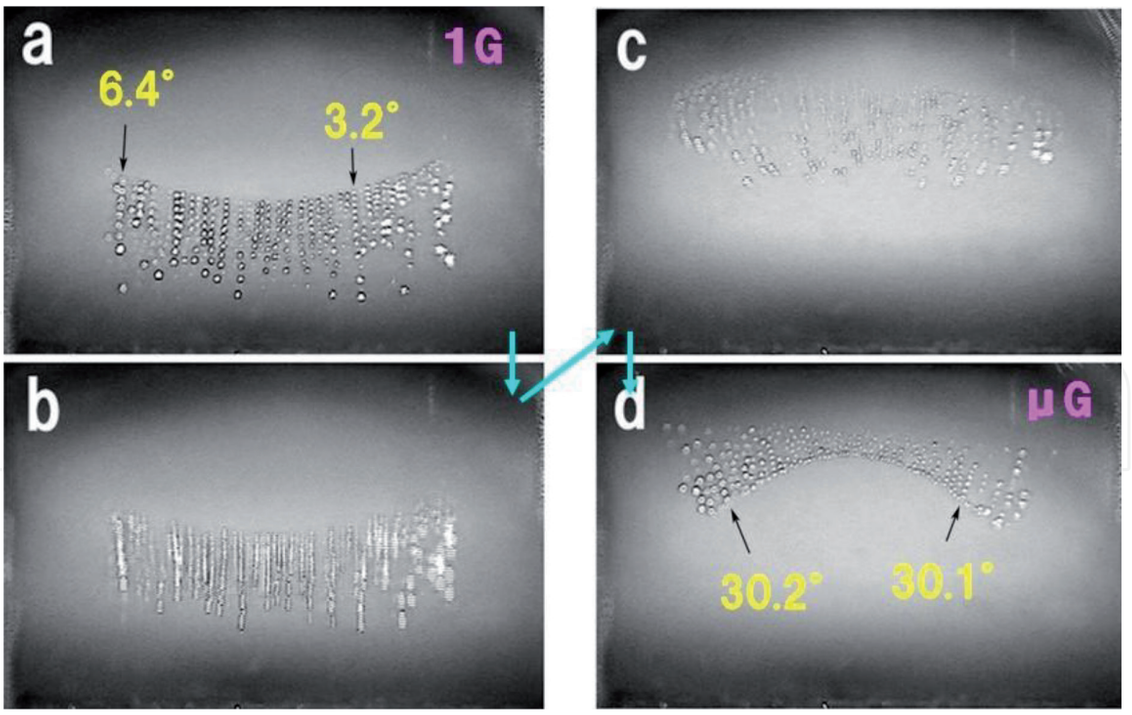

Figure 14.
Evolutions of ordering of fine particles during drop experiment: (a) just before drop under 1 g; (b) 2/30 s after beginning of drop; (c) 6/30 s after; (d) 3 s after. Directions of fine-particles alignment and tilt angles are indicated in (a) and (d). The height and width of the figures are 14 mm and 21 mm, respectively [38].

drop under gravity shows fine particles aligning in a nearly vertical direction. The image obtained 2/30 s after the beginning of the drop shows the fine particles going straight up in the vertical direction, while the 6/30 s image shows the particles radially moving upward. In 1.5-s movie, the movement slowed down and the alignment of the fine particles was observed again, however, it was not vertical but radial. Fine particles aligned in radial directions are seen in the image shown at 3 s in **Figure 14**.

The alignment of fine particles in the sheath should be caused by the effect of the formation of the wake field [18, 19]. The reason why the fine particles moved up after the beginning of the drop is due to the change in the balance of forces. Fine particles are suspended around the balance position of the resultant force (F for upward direction), which is composed of ion drag (f_I), electrostatic (f_E), and gravitational (f_G) forces under gravity, while they are around the position of balance induced by the former two forces (f_I and f_E) under zero gravity. Thus fine particles remain around the lower plasma-sheath boundary under gravity with the condition $F = f_E - f_I - f_G = 0$, and they are pushed upward there when gravity is diminished with the condition $F = f_E - f_I > 0$. The ion drag force directed toward the electrodes is larger than the electrostatic force toward the center of the plasma under the conditions of this experiment, when the ion-particle cross section is calculated with the impact parameter beyond the Debye length [39–41]. Because the mean free path of helium atoms or ions at the pressure of 133 Pa is 130 μm, which is much longer than the ion Debye length, the collisionless limit [41] is applicable to this experiment. As a result, the upward resultant force F changes and fine particles are pushed upward to the position near the upper grounded electrode passing over the center as shown in **Figure 15**. The force was calculated for a particle of the same size and weight as those used in the experiment and under similar plasma conditions [40]. In the calculation, the gravitational force f_G was 0.7×10^{-13} N, and the ion drag and electrostatic forces at the balance positions under gravity (1 G) were about 9.6×10^{-13} N and 10.3×10^{-13} N, respectively, for the charge of the isolated fine particle of 7340 e, which was evaluated under the

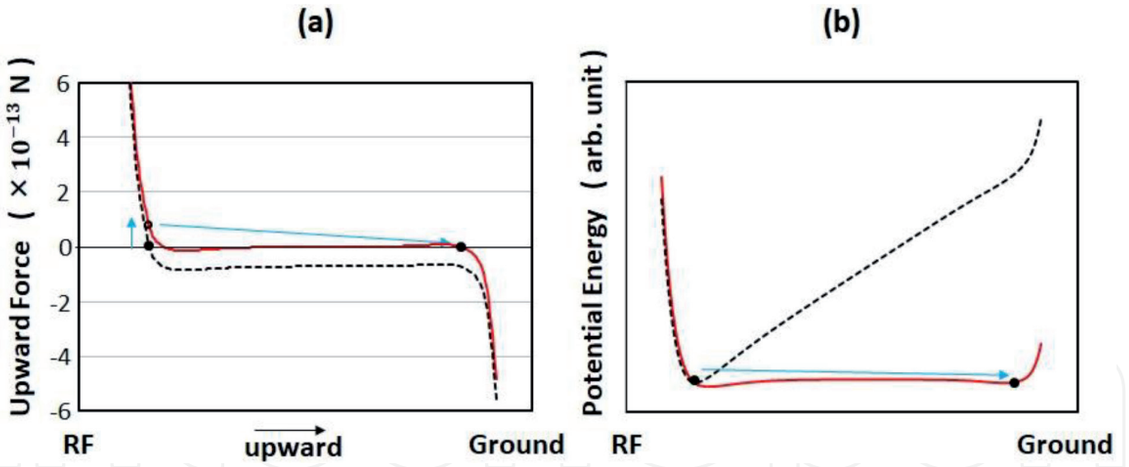

Figure 15.
Illustration of upward resultant force composed of ion drag, electrostatic and gravitational forces and behavior of fine particle in drop experiment under 1 G (black broken curve) to 0 G (red solid curve) (a); potential energy calculated from integral of curves of the resultant force in (a) (b). Closed circles show force balance position under 1 G and upper position under 0 G; open circle shows upward force under 0 G at the position of force balance under 1 G.

same plasma conditions as this experiment. The difference between the electrostatic and ion drag forces, $f_E - f_I = f_G = 0.7 \times 10^{-13}$ N, pushed the fine particles upward at the moment of gravitational change. Fine particles moved to a position around the upper plasma-sheath boundary beyond the unstable zero-resultant position if the upward force was sufficiently large for fine particles to pass through the center of the plasma.

Using the images shown in **Figure 14** along with images taken at the same time with the X-axis video camera, three-dimensional particle position coordinates were obtained. Three-dimensional tilt angles were determined for six inner particles to be 6.4°and 3.2°for the left and right rows in **Figure 14(a)**, and 30.2° and 30.1° for those in **Figure 14(d)**, respectively. Interparticle distances between the inner first and second particles were 320 and 230 μm for the left and right rows in **Figure 14(a)**, and 280 and 180 μm for those in **Figure 14(d)**, respectively, and the Mach numbers of ion speed were calculated to be in the range from 1.2 to 1.6.

Since the structure of the RF plasma system is symmetric both vertically and horizontally, the shape of plasma generated in the plastic cylinder is supposed to be symmetric, that is, spheroidal, when the sheath thickness is comparable to the order of plasma size. Therefore, under zero gravity, fine particles are subjected to a resultant force in the spheroidal plasma, that is, they are affected by the positive ion flow and electric field whose directions are radial. If the wake field theory is accepted here, the radial alignment of fine particles can be reasonably understood as being due to the formation of rows in the direction of ion flow. On the other hand, the vertical alignment of fine particles under gravity cannot be explained with the assumption of a spheroidal plasma. In order to determine the shape of the plasma, we analyzed the density distribution of the plasma containing fine particles and drew 16 contours through the division of optical emission brightness on CCD images. As is shown in **Figure 16**, the plasma was lowered and flattened under gravity compared to that under microgravity. The results suggest that fine particles suspended around the lower plasma-sheath boundary deformed the plasma.

By the effect of plasma wake [18, 19, 42], a negatively charged fine particle forms a positive potential in the downstream position of ion flow, and another fine particle is attracted to the position of maximum potential. At the same time, the gravitational force pulls the downstream fine particle down from its position [43]. The third downstream fine particle that is downstream to the second one is also

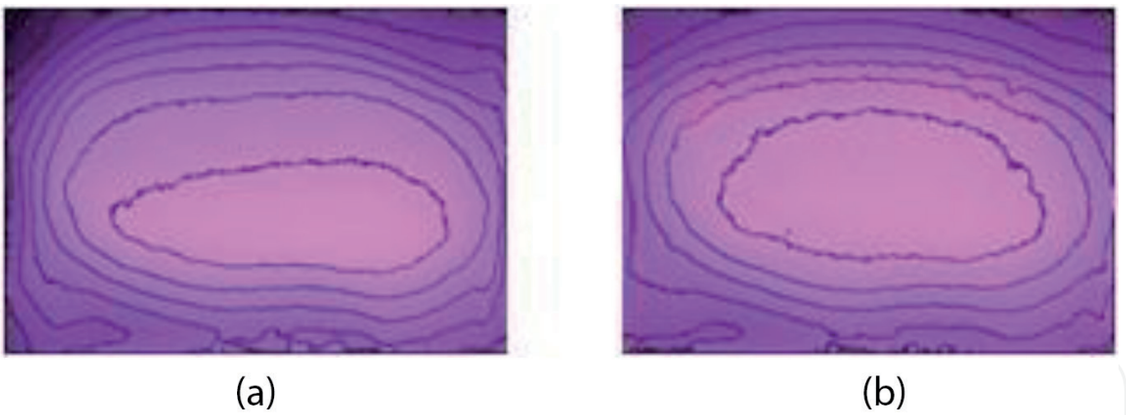

Figure 16.
Contours of intensity distribution of optical emission from plasma containing fine particles under 1 G (a) and microgravity (b). The height and width of the figures are 14 mm and 19 mm, respectively. [38].

pulled down by gravity to a position lower than that of maximum potential. Such force actions are repeated on other particles further downstream. Due to the sinking of the fine particles under gravity, ion flow is affected by the negative potential formed by fine particles in turn and tends to be vertically directed lowering the free energy. As a result, under gravity, the mutual influence between the positive ion flow and the negative fine particles results in the alignment being more vertical and in the deformation of the plasma. The reason why fine particles moved straight up in the vertical direction, as shown in the 2/30 s image of **Figure 14(b)**, is considered to be that the resultant force due to ion flow and the electric field was directed vertically upward just immediately after the diminishment of gravity.

Using the same plasma system that was used for drop experiment, a microgravity experiment by parabolic flight was carried out under the condition of less than 0.04 G in the vertical direction and less than 0.01 G in the horizontal direction for approximately 20 s at the Diamond Air Service Inc. in Japan. The plasma system was installed in a standardized rack in a jet plane. **Figure 17** shows the images of fine particle behavior taken by the Y-axis video camera during the changes in gravitational conditions from 2 G (a) to microgravity (c) and to 1.5 G (e). Under microgravity, in **Figure 17(c)**, fine particles are also observed around the lower balance position forming a void in the center as was reported [44]. The number of injected fine particles was approximately 10 times greater than that for the drop experiment. Most of the fine particles were pushed to the upper balance region at the moment of gravitational change, however, some remained behind due to their mutual Coulomb repulsive forces. In addition, fine particles injected continuously during the microgravity condition were also suspended around the lower balance position. Fine particles at the inner boundary were arranged parallel to the electrodes under gravity more than 1 G, while they formed an arc under microgravity even around the lower plasma-sheath boundary. In transition from 2 G to microgravity (b), the fine particles moved vertically upward. On the other hand, in transition from microgravity to 1.5 G (d), they moved downward through the outer side of the plasma and a void was formed in the center. The nonsymmetrical behavior of fine particles in transition can be explained by the difference in the state of plasma containing fine particles. As explained above concerning the results of the drop experiment, the resultant of ion drag and electrostatic forces pushed the fine particles vertically upward at the moment shown in **Figure 17(b)**. However, the particles were obliquely pulled down during the increase of gravity as shown in **Figure 17(d)** by the oblique force that is composed of the gravitational force and the outward radial force, which is derived from the ion drag force stronger than the electrostatic force.

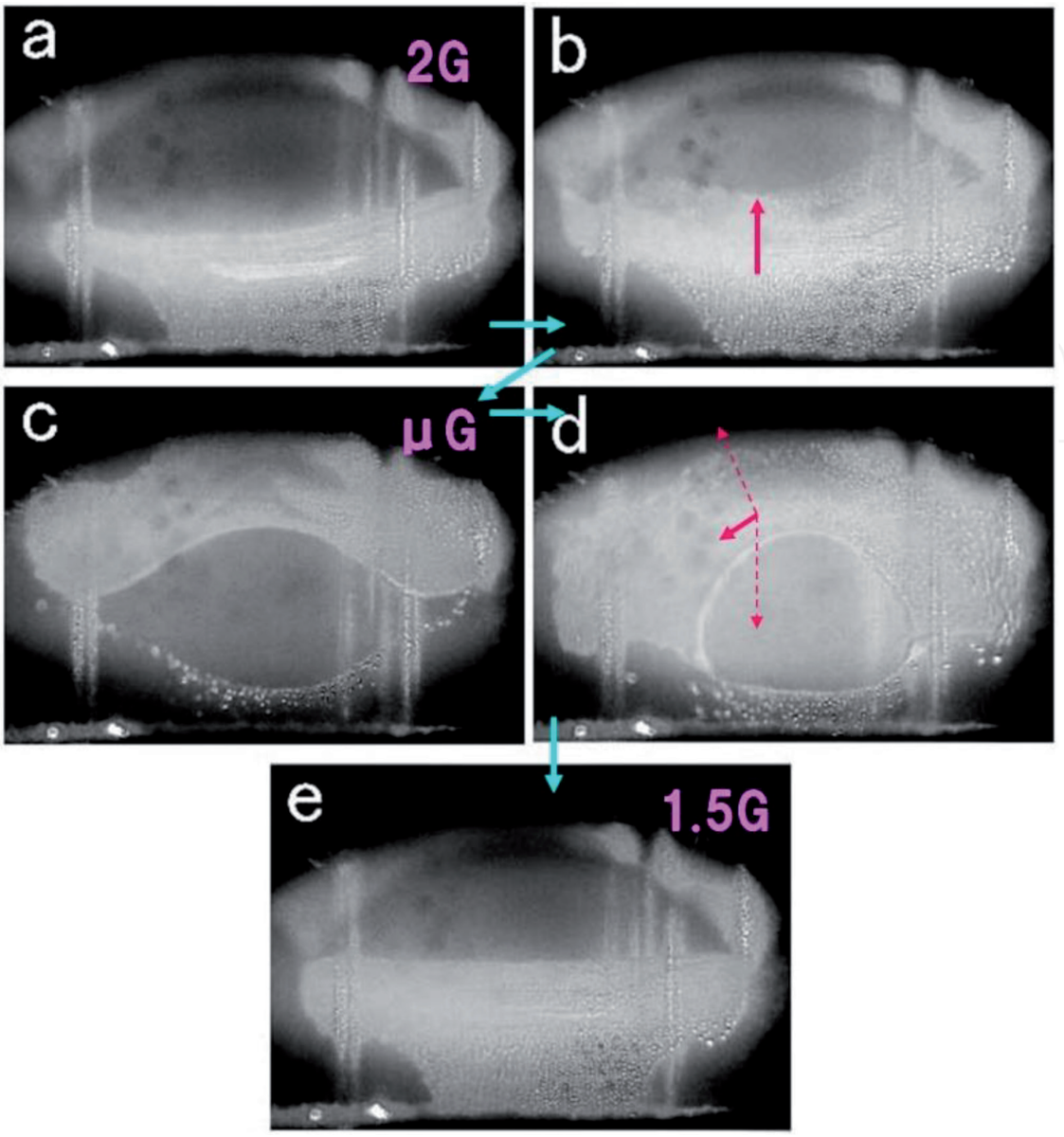

Figure 17.
Video images of fine particle behavior in parabolic flight under gravitational conditions: (a) 2 G, (b) transition from 2 G to microgravity, (c) microgravity, (d) transition from microgravity to 1.5 G and (e) 1.5 G. In the case of (a), fine particles were accelerated by 0.1–0.2 G in the right direction of the image [38].

Such "void" was observed in the center of plasma under microgravity condition performed on the International Space Station (ISS) [45]. The cause of "void" formation is generally considered to be due to strong ion drag force at the center of plasma [39–41].

5. Conclusions

The observation of Coulomb crystals in fine particle plasmas was presented in this chapter. Their 3D crystal structures were fcc, fco, and bct, but bcc structure have not been observed. The latter result is due to the fact that the rearrangement from fcc to fco or bct occurs with constant particle density in horizontal planes and with interplane vertical distance constant. It is explained that the crystal structure was formed from the pile of the plain layers perpendicular to the direction of an external force with constant interplane distance being arranged by the secondary effect of the Coulomb force of particles in nearby layers to minimize the average Coulomb energy.

The structure change of Coulomb crystal during the growth of carbon particles was observed and analyzed with the use of Mie-scattering ellipsometry. The arrangement of fine particles 1.3 μm in diameter showed 3D regularity, while that of diameter 2.2 μm formed 2D close-packed crystal structure.

The spatial distribution of size of particles forming horizontal layers was analyzed by Mie-scattering ellipsometry using an image sensor. By the comparison of the determined values Ψ and Δ with calculation, particle diameter was evaluated to be 2.70, 2.74, 2.75, and 2.77 μm for particles in upper to lower layers. Its diameter was determined with accuracy as low as 0.01 μm (10 nm). Such measurement method may be useful for the analysis of phase separation phenomena, which is observed in general materials, in fine particle plasmas.

3D Coulomb crystals in fine particle plasmas can be good models of real atomic crystal and its formation and melting processes. Thus physical phenomena in solid, liquid, and gas states, which are, for example, the liquid-to-solid phase transition [46, 47], critical phenomena [48], soliton [49], chaos [50], can be simulated and analyzed on the basis of observation of behavior of individual fine particles. Such an experimental method enables the kinetic analyses of component behavior in the study of statistical properties of a system, along with the complementary uses of the computer simulations of molecular dynamics (MD) or Monte-Carlo method (MC).

In order to analyze a 3D Coulomb crystal as a model of real atomic crystal, it is preferable to make its conditions of environment close to the real crystal. Spatially isotropic force field acting on fine particles is required for the conditions. Microgravity environment can eliminate unidirectional gravity; however, the resultant force of electrostatic and ion drag forces pushes fine particles outward from the center forming the void of them [44, 45]. The fabrication of a plasma system that does not generate such a void is yet an unresolved issue and that with homogeneous conditions is under development [51, 52].

Acknowledgements

The author thanks Prof. Kunihide Tachibana, Prof. Kazuo Takahashi, Prof. Akio Sanpei, Prof. Yukio Watanabe, Prof. Noriyoshi Sato, and members of the project of Plasma Control Science Research in Kyoto Institute of Technology for useful discussions. He also thanks laboratory students of Kyoto Institute of Technology for experimental assistance. This work was partly supported by the Ministry of Education, Science, Sports and Culture of Japan.

Author details

Yasuaki Hayashi
Kyoto Institute of Technology, Sakyo-ku, Kyoto, Japan

Address all correspondence to: hayashiy@kit.ac.jp

References

[1] Hayashi Y, Tachibana K. Observation of Coulomb-crystal formation from growing particles grown in a methane plasma. Japanese Journal of Applied Physics. 1994;**33**:L804-L806. DOI: 10.1143/JJAP.33.L804

[2] Chu JH, Lin I. Direct observation of Coulomb crystals and liquids in strongly coupled rf dusty plasmas. Physical Review Letters. 1994;**72**:4009-4012. DOI: 10.1103/PhysRevLett.72.4009

[3] Thomas H, Morfill GE, Demmel V, Goree J, Feuerbach B, Möhlmann D. Plasma crystal: Coulomb crystallization in a dusty plasma. Physical Review Letters. 1994;**73**:652-655. DOI: 10.1103/PhysRevLett.73.652

[4] Melzer A, Trottenberg T, Piel A. Experimental determination of the charge on dust particles forming Coulomb lattices. Physics Letters A. 1994;**191**:301-308. DOI: 10.1016/0375-9601(94)90144-9

[5] Ikezi H. Coulomb solid of small particles in plasmas. The Physics of Fluids. 1986;**29**:1764-1766. DOI: 10.1063/1.865653

[6] Ichimaru S. Strongly coupled plasma. High-density classical plasmas and degenerate electron liquids. Reviews of Modern Physics. 1982;**54**:1017-1059. DOI: 10.1103/RevModPhys.54.1017

[7] Alder BJ, Wainwright TE. Phase transition for a hard sphere system. Journal of Chemical Physics. 1957;**27**:1208-1209. DOI: 10.1063/1.1743957

[8] Wood WW, Jacobson JD. Preliminary results from a recalculation of the Monte Carlo equation of state of hard spheres. The Journal of Chemical Physics. 1957;**27**:1207-1208. DOI: 10.1063/1.1743956

[9] Alder BJ, Hoover WG, Young DA. Studies in molecular dynamics. V. High-density equation of state and entropy for hard disks and spheres. The Journal of Chemical Physics. 1968;**49**:3688-3699. DOI: 10.1063/1.1670653

[10] Brush SG, Sahlin HL, Teller E. Monte Carlo study of a one-component plasma. I. Journal of Chemical Physics. 1966;**45**:2102-2119. DOI: 10.1063/1.1727895

[11] Hoover WG, Gray WG, Johnson KW. Thermodynamic properties of the fluid and solid phases for inverse power potentials. Journal of Chemical Physics. 1971;**55**:1128-1136. DOI: 10.1063/1.1676196

[12] Robbins MO, Kremer K, Grest GS. Phase diagram and dynamics of Yukawa systems. Journal of Chemical Physics. 1988;**88**:3286-3312. DOI: 10.1063/1.453924

[13] Farouki RT, Hamaguchi S. Thermodynamics of strongly-coupled Yukawa systems near the one-component-plasma limit. II. Molecular dynamics simulations. Journal of Chemical Physics. 1994;**101**:9885-9893. DOI: 10.1063/1.467955

[14] Waki I, Kassner S, Birkl G, Walther H. Observation of ordered structures of laser-cooled ions in a quadrupole storage ring. Physical Review Letters. 1992;**68**:2007-2010. DOI: 10.1103/PhysRevLett.68.2007

[15] Mitchell TB, Bollinger JJ, Dubin DHE, Huang X-P, Itano WM, Baughman RH. Direct observations of structural phase transitions in planar crystallized ion plasmas. Science. 1998;**282**:1290-1293. DOI: 10.1126/science.282.5392.1290

[16] Dosho S et al. Recent studies of polymer latex dispersions. Langmuir.

1993;**9**:394-411. DOI: 10.1021/la00026a008

[17] Hayashi Y, Mizobata Y, Takahashi K. Behaviors of fine particles in a planar magnetron plasma. Journal of Plasma and Fusion Research Series. 2009;**8**:298-301

[18] Nambu M, Vladimirov SV, Shukla PK. Attractive forces between charged particles in plasmas. Physics Letters A. 1995;**203**:40-42. DOI: 10.1016/0375-9601(95)00380-L

[19] Melandso F, Goree J. Polarized supersonic plasma flow simulation for charged bodies such as dust particles and spacecraft. Physical Review E. 1995;**52**:5312-5326. DOI: 10.1103/PhysRevE.52.5312

[20] Totsuji H, Kishimoto T, Totsuji C. Structure of confined Yukawa system (dusty plasma). Physical Review Letters. 1997;**78**:3113-3116. DOI: 10.1103/PhysRevLett.78.3113

[21] Hayashi Y. Structural transitions of 3-dimensional Coulomb crystals in a dusty plasma. Physica Scripta. 2001;**T89**:112-116. DOI: 10.1238/Physica.Topical.089a00112

[22] Hayashi Y, Tachibana K. Analysis of spherical carbon particle growth in methane plasma by Mie-scattering ellipsometry. Japanese Journal of Applied Physics. 1994;**33**:4208-4211. DOI: 10.1143/JJAP.33.4208

[23] Hayashi Y. Structure of a three-dimensional Coulomb crystal in a fine-particle plasma. Physical Review Letters. 1999;**83**:4764-4767. DOI: 10.1103/PhysRevLett.83.4764

[24] Nishiyama Z. X-ray investigation the mechanism of transformation from face-centered-cubic lattice to body-centered cubic. Science Report Tohoku University. 1934;**23**:637-664

[25] Mie G. Beiträge zur Optik trüber Medien, speziell kolloidaler Metallösungen. Annalen der Physik. 1908;**25**:377-445. DOI: 10.1002/andp.19083300302

[26] Born M, Wolf E. Principles of Optics. 5th ed. Oxford: Pergamon; 1975. Section 13.5

[27] van de Hulst HC. Light Scattering by Small Particles. New York: Dover; 1981. 470 p

[28] Tachibana K, Hayashi Y, Okuno T, Tatsuta T. Spectroscopic and probe measurements of structures in a parallel-plates RF discharge with particles. Plasma Sources Science and Technology. 1994;**3**:314-319. DOI: 10.1088/0963-0252/3/3/012

[29] Watanabe Y, Shiratani M, Yamashita M. Observation of growing kinetics of particles in a helium-diluted silane rf plasma. Applied Physics Letters. 1992;**61**:1510-1512. DOI: 10.1063/1.107532

[30] Hayashi Y, Tachibana K. Mie-scattering ellipsometry for analysis of particle behaviors in processing plasmas. Japanese Journal of Applied Physics. 1994;**33**:L476-L478. DOI: 10.1143/JJAP.33.L476

[31] Born M, Wolf E. Principles of Optics. 5th ed. Oxford: Pergamon; 1975. Section 10.8

[32] Hayashi Y, Sanpei K. Mie-scattering Ellipsometry. In: Wahaia F, editor. Ellipsometry. Rijeka, Chapter: IntechOpen; 2017. p. 1. DOI: 10.5772/65558

[33] Hayashi Y. Measurement of fine-particles by Mie-scattering ellipsometry. Journal of The Vacuum Science of Japan. 2001;**44**:617-623. DOI: 10.3131/jvsj.44.617

[34] Hayashi Y, Takahashi K. Structural changes of Coulomb crystal in a carbon fine-particle plasma. Japanese Journal of Applied Physics. 1997;**36**:4976-4979. DOI: 10.1143/JJAP.36.4976

[35] Hayashi Y, Kawano M, Sanpei A, Masuzaki S. Mie-scattering ellipsometry system for analysis of dust formation process in large plasma device. IEEE Transactions on Plasma Science. 2016;**44**:1032-1035. DOI: 10.1109/TPS.2016.2542349

[36] Hayashi Y, Sanpei A, Mieno T, Masuzaki S. Analysis of spatial distribution of fine particles in plasma by imaging Mie-scattering ellipsometry. In: 8th International Conference on the Physics of Dusty Plasmas; May 20-25, 2017; Prague, Czech Republic. 2017

[37] Barnes MS, Keller JH, Forster JC, O'Neil JA, Coultas DK. Transport of dust particles in glow-discharge plasmas. Physical Review Letters. 1992;**66**:313-316. DOI: 10.1103/PhysRevLett.68.313

[38] Hayashi Y. Radial ordering of fine particles in plasma under microgravity condition. Japanese Journal of Applied Physics. 2005;**44**:1436-1440. DOI: 10.1143/JJAP.44.1436

[39] Kilgore MD, Daugherty JE, Porteous RK, Graves DB. Ion drag on an isolated particulate in a low-pressure discharge. Journal of Applied Physics. 1993;**73**:7195-7202. DOI: 10.1063/1.352392

[40] Hayashi Y, Takahashi K, Sato H. Analyses of particle behaviors and formation of Coulomb crystals in plasmas. Journal of The Vacuum Science of Japan. 1998;**41**:782-789. DOI: 10.3131/jvsj.41.782

[41] Khrapak SA, Ivlev AV, Morfill GE, Thomas HM. Ion drag force in complex plasmas. Physical Review E. 2002;**66**: 1-4. DOI: 10.1103/PhysRevE.66.046414

[42] Takahashi K, Oishi T, Shimomai K, Hayashi Y, Nishino S. Analyses of attractive forces between particles in Coulomb crystal of dusty plasmas by optical manipulations. Physical Review E. 1998;**58**:7805-7811. DOI: 10.1103/PhysRevE.58.7805

[43] Takahashi K, Oishi T, Shimomai K, Hayashi Y, Nishino S. Simple hexagonal Coulomb crystal near a deformed plasma sheath boundary in a dusty plasma. Japanese Journal of Applied Physics. 1998;**37**:6609-6614. DOI: 10.1143/JJAP.37.6609

[44] Morfill GE, Thomas HM, Konopka U, Rothermel H, Zuzic M, Ivlev A, et al. Condensed plasmas under microgravity. Physical Review Letters. 1999;**83**:1598-1601. DOI: 10.1103/PhysRevLett.83.1598

[45] Nefedov AP et al. PKE-Nefedov: Plasma crystal experiments on the international Space Station. New Journal of Physics. 2003;**5**:33.1-33.10

[46] Thomas HM, Morfill GE. Melting dynamics of a plasma crystal. Nature. 1996;**379**:806-809. DOI: 10.1038/379806a0

[47] Krapak SA et al. Fluid-solid phase transition in three-dimensional complex plasmas under microgravity conditions. Physical Review E. 2012;**85**:1-11. DOI: 10.1103/PhysRevE.85.066407

[48] Totsuji H, Takahashi K, Adachi S, Hayashi Y, Takayanagi M. Strongly coupled plasmas under microgravity. International Journal of Microgravity Science and Application. 2011;**28**:S27-S30

[49] Sheridan TE, Nosenko V, Goree J. Experimental study of nonlinear solitary waves in two-dimensional dusty plasma. Physics of Plasmas. 2008;**15**:1-6. DOI: 10.1063/1.2955476

[50] Lin I, Juan W, Chiang C, Chu JH. Microscopic particle motions in strongly coupled dusty plasmas. Science. 1996;**272**:1626-1628. DOI: 10.1126/science.272.5268.1626

[51] Arp O, Block D, Piel A, Melzer A. Dust Coulomb balls: Three-dimensional plasma crystals. Physical Review Letters. 2004;**93**:1-4. DOI: 10.1103/PhysRevLett.93.165004

[52] Thomas HM, Knapek C, Huber P, Mohr DP, Zähringer E, Molotkov V, et al. Ekoplasma—The Future of Complex Plasma Research in Space. 2017. Available from: https://core.ac.uk/display/86640180